ACS Sustainable Chemistry & Engineering

pubs.acs.org/journal/ascecg

Research Article

Predicting the Thermal Behavior in the Design of Type V Deep Eutectic Solvents: The Combined Role of Polarity and Steric Asymmetry

Giorgia Mannucci, Gabriel Teixeira, Filipe Hobi Bordon Sosa, Matteo Palluzzi, Matteo Busato, João A. P. Coutinho,* and Paola D'Angelo*

Cite This: https://doi.org/10.1021/acssuschemeng.3c07965

Read Online

ACCESS | Metrics & More | Article Recommendations | Supporting Information

ABSTRACT: The thermal behavior of the hydrophobic eutectic mixtures formed by L-menthol (MEN) with 4-methoxyphenol (4-Met), 2-*tert*-butyl-4-methoxyphenol (BHA), 2-*tert*-butyl-4-ethylphenol (TBEP), and *tert*-butylhydroquinone (TBHQ) has been investigated to elucidate the different factors governing the solid–liquid equilibrium (SLE) at the molecular level. Our comparative study highlights the contribution of hydrogen-bonding (H-bonding) asymmetry of deep eutectic solvent (DES) precursors, i.e., their ability to act as strong H-bond donors and weak H-bond acceptors or vice versa. When deriving from resonance effects, this concept was previously presented as "polarity asymmetry" and introduced to explain the thermal behavior of type V DES. Here, we expand this concept to demonstrate that steric factors led by the insertion of ad hoc functional groups in the precursor molecules also have a dominant role in the deviation from thermodynamic ideality. In this way, an increasing temperature depression is observed starting from the 4-Met/MEN mixtures up to the BHA/MEN, TBHQ/MEN, and TBEP/MEN ones. The SLE prediction has been carried out through an innovative approach combining the COSMO-RS solvation model and density functional tight-binding molecular dynamics simulations, benchmarked against experimental data, and presented here for the first time. The impact of this work is that of providing new tools for a more conscious understanding and design of hydrophobic type V DES as new sustainable media for applicative purposes.

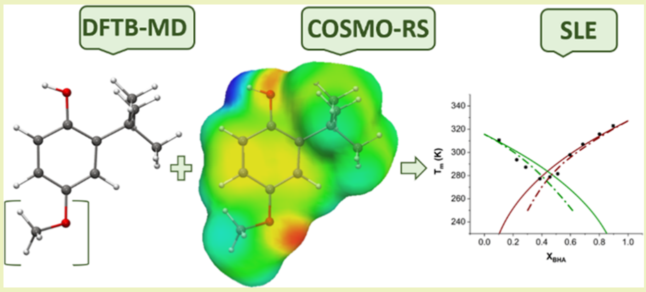

KEYWORDS: *deep eutectic solvents, hydrophobic, menthol, COSMO-RS, molecular dynamics, DSC, SLE*

■ INTRODUCTION

Deep eutectic solvents (DESs) are a peculiar class of novel green media that have recently attracted a lot of attention due to their distinct chemical-physical properties. In many cases, these solvents show nonflammability, low vapor pressure, reduced toxicity, and high solvating capability.[1−3] As a result, they are well suited for a variety of applications, including the extraction of metal species,[4,5] biomolecules,[6] pesticides,[7,8] and medicinal components from aqueous solutions,[9] energy production and storage,[10,11] electroplating,[12−14] and catalytic processes,[15,16] among others. At variance with traditional solvents, which are pure substances, DESs are prepared by mixing at least two precursor compounds, often solid at room temperature. This opens a wide horizon of opportunities since by judicious choice of the precursors and their molar ratio, or through an appropriate functionalization of the parent molecules, one may directly act on the DES chemical-physical properties, so that these media sit by right in the realm of the "designing" solvents.[17−20] It is widely accepted that DES classification relies on the chemical nature of the parent compounds and they are divided into five categories (I–V).[3]

Differently from types I–IV, which are composed by at least one ionic component, the more recent type V DESs are formed by neutral molecular compounds, only. Being nonionic, DESs belonging to this family typically display lower viscosities, are chloride-free and often hydrophobic. Indeed, hydrophobic deep eutectic solvents (HDESs) have drawn significant attention as a greener alternative to conventional media for liquid–liquid biphasic extractions of several target compounds from aqueous solutions.[21−23]

The solid–liquid equilibrium (SLE) between the precursors is at the basis of DES formation since it brings to the eutectic-type behavior and hopefully to the achievement of a liquid phase at the operating temperature. Despite this being typical of every eutectic, DESs are defined so that the melting point

Received: December 4, 2023
Revised: January 19, 2024
Accepted: January 22, 2024

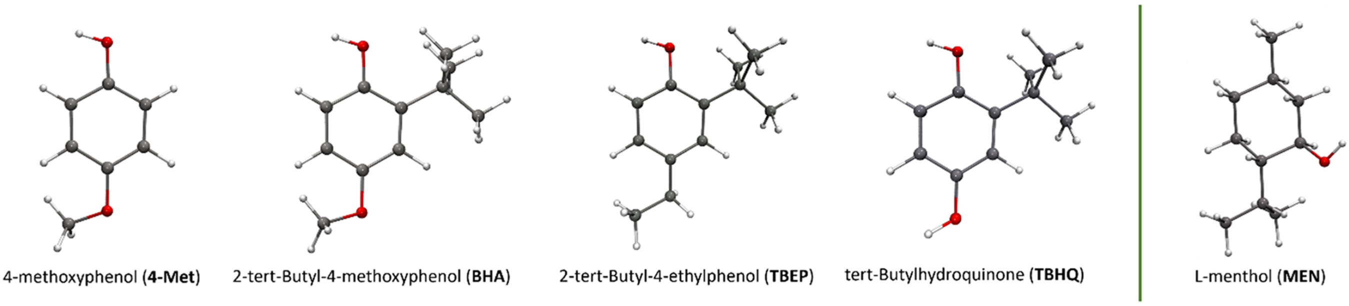

Figure 1. Molecular structures of 4-methoxyphenol (4-Met), 2-*tert*-butyl-4-methoxyphenol (BHA), *tert*-butylhydroquinone (TBHQ), 2-*tert*-butyl-4-ethylphenol (TBEP), and L-menthol (MEN) (white: hydrogen; gray: carbon; red: oxygen).

(MP) depression is significantly deeper than the one predicted assuming thermodynamic ideality for at least one of the compounds across the SLE phase diagram.[24] Nevertheless, the amount of MP depression to provide a "true" DES instead of an ideal eutectic is still controversial, so that this view has been challenged repeatedly.[25]

From a thermodynamic perspective, the MP depression originates when the interactions between the mixed components are stronger than in their precursor's pure form. The nature of such interactions has almost always been attributed to hydrogen-bonding (H-bonding),[1,26,27] so that the precursors are often indicated as H-bond donor (HBD) and H-bond acceptor (HBA) species. To obtain a significant deviation from ideality, one may therefore desire the noncovalent interactions among the parent molecules in the liquid phase of the pure state to be as weak as possible while being maximized in the mixed state. This can be achieved with compounds having strong HBD and weak HBA functionalities or vice versa, a condition which was previously indicated as "polarity asymmetry". This concept was already introduced to explain the thermal behavior of the archetypal type V DES formed by thymol and L-menthol (MEN).[28,29] In fact, the thymol hydroxyl group is more positive due to resonance effects, which makes the hydrogen atom a stronger HBD but the oxygen atom a weaker HBA with respect to nonphenolic species. The effect is that it hampers the self-aggregation among thymol molecules in the pure state. On the other hand, no resonance effects are present in the MEN molecule. Thus, upon mixing of the two compounds, the thymol molecule can establish with MEN stronger H-bonds than in its pristine form, leading to the deviation from thermal ideality. Note that a remarkable MP depression is highly desirable since it can disclose a higher composition versatility of the mixture, meaning that the precursor molar ratio can be deliberately changed to achieve the desired chemical-physical properties without losing the liquid window. As a result, it is of great interest to expand the existing knowledge about the thermal behavior of these mixtures to correlate the deviation from ideality to their structural and electronic properties.

Inspection of the entire SLE phase diagram is an important step to characterize a eutectic mixture.[25] This is typically achieved by measuring the melting temperature (T_m) of the mixture for different molar fractions of the parent compounds with thermal methods, such as differential scanning calorimetry (DSC). However, these experiments can represent a considerable effort in term of resources and/or be affected by problems of the sample such as lack of crystallization or cocrystal formation for some compositions.[30] In this sense, the demand for predictive methodologies has recently grown, resulting in an increased usage of computational approaches as a screening tool to drive the experimental design of type V DES. The most popular methods for SLE determination are those based on the COSMO solvation model, such as COSMO-RS and COSMO-SAC,[31−35] that are based on the calculation of the activity coefficients combining statistical thermodynamics with quantum chemical descriptors.[36−38] However, these techniques benefit substantially from comparison with experimental data, and therefore, there is a need for the improvement of these computational approaches and for the development of more reliable predictive methodologies.

Here, we present a comprehensive study of the thermal behavior of the hydrophobic eutectic mixtures formed by L-menthol with 4-methoxyphenol (4-Met), 2-*tert*-butyl-4-methoxyphenol (BHA), 2-*tert*-butyl-4-ethylphenol (TBEP), and *tert*-butylhydroquinone (TBHQ). MEN is widely found in type V DESs because of its inherent sustainability and availability from natural sources, and consequently, the study of its mixtures is of great interest.[39] Furthermore, inspection of the molecular structures of the selected counterpart compounds (Figure 1) delivers the key to this study, that is, investigating how the presence of different functional groups can affect the H-bonding capability and ultimately the mixture liquid window of these systems. To this purpose, the COSMO-RS model was used to predict the SLE phase diagram, and the results obtained using different quantum chemical levels were compared. To increase the accuracy of the predictions, the SLEs were also computed taking into account the relative abundance of the component molecule rotational conformers, calculated from density functional tight-binding molecular dynamics (DFTB-MD) simulations. With the purpose of validating this combined approach, which we present here for the first time, the theoretical predictions were compared step-by-step with the experimental data obtained by DSC measurements.

■ MATERIALS AND METHODS

Chemicals and Sample Preparation. MEN (natural source, food grade, ≥99%), 4-Met (≥97%), BHA (≥90%), and TBHQ (≥97%) were purchased from Merck Life Science S.r.l. (Milan, Italy), while TBEP (≥98%) was purchased from BLD Pharmatech GmbH. 4-Met/MEN, BHA/MEN, TBEP/MEN, and TBHQ/MEN mixtures at different molar fractions of the components, $x_{4\text{-Met}}$, x_{BHA}, x_{TBEP}, and x_{TBHQ}, respectively, were prepared by mixing the desired amount of the compounds in a glass test tube and then heating until homogeneous liquids were obtained. The full list of the prepared samples is reported in Tables S1−S4 of the Supporting Information.

Solid−Liquid Equilibrium Measurements. A PerkinElmer AD6 microanalytical balance, a Hitachi DSC7000X working at atmospheric pressure and coupled with an electrical cooling unit, and a Mettler-

https://doi.org/10.1021/acssuschemeng.3c07965
ACS Sustainable Chem. Eng. XXXX, XXX, XXX−XXX

Toledo DSC 821 in a 70 mL/min nitrogen flux were used. Samples of approximately 5 mg were weighted, sealed in hermetic aluminum crucibles, and heated at a rate of 2 K min^{-1} under nitrogen atmosphere. A baseline was also determined with an empty sample holder to eliminate the effect of the gas. The equipment was calibrated with several standards (decane, 4-nitrotoluene, naphthalene, benzoic acid, diphenylacetic acid, indium, tin, caffeine, lead, zinc, potassium nitrate, water, and anthracene) at 2 K min^{-1}. First, the samples were cooled to 193.15 at 10 K min^{-1} and then heated at 2 K min^{-1} until complete melting. Since some of the mixtures presented cold crystallization phenomena, a procedure was applied of at least two heating steps (at 2 K min^{-1}) until before the eutectic temperature or 20 K above the glass transition and cooling steps (at 10 K min^{-1}) until 5 K above the glass transition. This procedure attempted to ensure completion of the crystallization transition, which was not always evident. Then, the last heating step at 2 K min^{-1} was performed for thermal analysis until the complete melting. The MP of each mixture was taken as the maximum value of the melting peak, as shown in Figure S1 for the 4-Met/MEN system, as an example.

For the mixtures in the solid state at room temperature, the melting temperature was determined via a "visual method" by means of an automatic glass capillary device, model M-565 from Büchi (Flawil, Switzerland), with a temperature resolution of 0.1 K, which was used to measure the melting temperature. The samples were loaded into melting point capillaries at room temperature and heated until the phase transition was observed. At least three independent measurements were made by applying a heating rate of 0.2 or 0.1 K min^{-1}. A complete list of the measurements is reported in Tables S1−S4 of the Supporting Information.

COSMO-RS. The MEN, 4-Met, BHA, TBEP, and TBHQ molecules were optimized by density functional theory (DFT) calculations with the TURBOMOLE V4.5.2 package,[40] using the COSMO solvation model with infinite permittivity, the B-P86 functional[41,42] and the def_TZVP[43] or def2_TZVPD[44,45] basis set. The COSMOtherm21[46] software was used to perform all COSMO-RS related calculations. First, the results obtained using the BP_TZVP_21 and BP_TZVPD_FINE_21 parametrizations were compared. Second, the calculation of the SLE phase diagrams was carried out by inserting a weight factor (*wf*) to include the conformer percentage yield from DFTB-MD simulations (vide infra). In Figure S2, the molecular structures of the *cisoid* and *transoid* conformers of the BHA, TBEP, and TBHQ components are represented. The experimental thermal properties for the pure components employed for SLE calculations and the *wf* employed are reported in Tables S5 and S6, respectively. Note that the employed conformer populations were extracted from DFTB-MD simulations at a definite temperature (Table S7) and kept constant during the SLE calculations since we observed a change lower than 5% of these populations across the explored temperature range. The deviation from thermal ideality was quantified as the difference between the MP calculated for the ideal liquid phase model and that obtained from the COSMO-RS calculations both taken at the eutectic composition (Table S8).[25]

Computational Details. The third order variant of the density functional tight-binding (DFTB3) level of theory, which has previously been shown to improve the description of H-bond interactions,[47−49] was used for the DFTB-MD simulations of the BHA, TBEP, and TBHQ compounds using the DFTB+21.2 program[50] in combination with the third-order-parametrization for organic and biological systems (3OB) Slater-Koster files.[51] Cubic boxes with ∼20 Å side lengths and a number of species chosen to reproduce the density of each system were built by randomizing the initial atomic positions with the PACKMOL package.[52] Details about the studied systems are reported in Table S7. After geometry optimization, a 2 ps NVE run and 10 ps NVT equilibration at 600 K were carried out, followed by 50 ps of a production run at a temperature above the MP of each system (Table S7). A Nosé−Hoover thermostat with a coupling strength of 3200 cm^{-1} was used to achieve thermalization. The velocity Verlet algorithm, with a 1.0 fs time step, was used to integrate the equations of motion, and trajectories were saved every 10 steps. Periodic boundary conditions were applied in all directions. The *k*-points mesh corresponded to a Γ-point sampling, while self-consistent charge optimization was carried out with 10^{-5} tolerance. Grimme's DFT-D4 empirical dispersion corrections were applied to improve the description of van der Waals interactions.[53]

The density of the TBHQ compound at 408 K was estimated by means of a classical MD simulation in the NPT ensemble carried out for 10 ns at 1 atm with the Gromacs 2020.6 program.[54] Structures and interactions of the TBHQ molecules were represented by the all-atom optimized potentials for liquid simulations (OPLS-AA) force field.[55] The long-range electrostatic forces were calculated with the particle mesh Ewald method[56,57] and a cutoff radius of 9 Å was chosen for all the nonbonded interactions. Cross-terms for the Lennard-Jones interactions were constructed with the Lorentz−Berthelot combining rules. The Nosé-Hoover thermostat with a relaxation constant of 0.5 ps and a Parrinello-Rahaman barostat with a coupling constant of 1.0 ps were employed. The leapfrog algorithm was used to integrate the equation of motion with a time step of 1.0 fs. The LINCS algorithm[58] was employed to constrain all the stretching vibrations involving the hydrogen atoms.

An analysis population was carried out for the 4-Met, BHA, TBEP, TBHQ, and MEN molecules by calculating the partial charges with the CHELPG scheme.[59] To this purpose, geometry optimizations of the isolated molecules in gas phase conditions were carried out at DFT level using the B3LYP functional[60] in combination with the def2_TZVP basis set.[44,45] The GAUSSIAN 16 package[61] was used for DFT simulations.

RESULTS AND DISCUSSION

Setting Up the Predictive Method: 4-Met/MEN and BHA/MEN. In Figure 2a, we report the simulated SLE phase diagram for the 4-Met/MEN mixture calculated with the COSMO-RS BP_TZVP_21 parametrization, compared with the phase diagram traced assuming thermodynamic ideality and the obtained experimental melting temperatures. Despite this level of theory being previously used with success for the thermal characterization of DESs,[62−64] here it can be observed

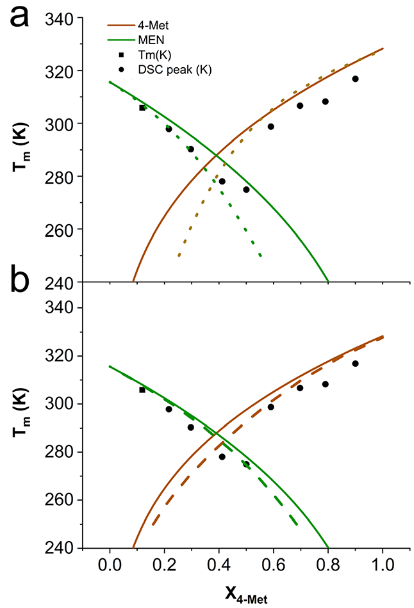

Figure 2. Experimental SLE phase diagram for the 4-Met/MEN system measured using DSC (black circle) and the visual method (black square). Predictions obtained by the ideal liquid phase model (solid lines) and COSMO-RS theoretical curves calculated using the BP_TZVP_21 (dotted lines) (a) and BP_TZVPD_FINE_21 (dashed lines) (b) parametrizations.

https://doi.org/10.1021/acssuschemeng.3c07965
ACS Sustainable Chem. Eng. XXXX, XXX, XXX−XXX

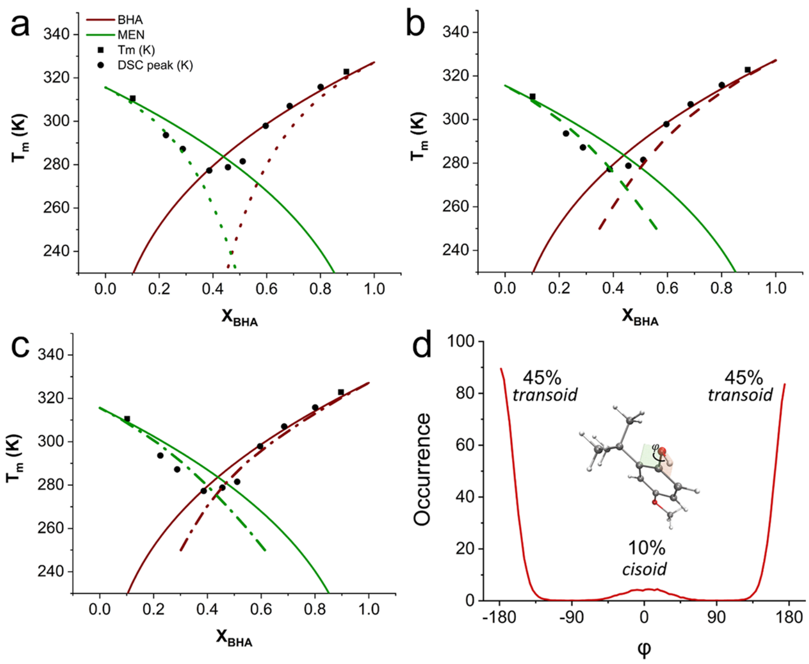

Figure 3. Experimental SLE phase diagram for the BHA/MEN system measured using DSC (black circle) and the visual method (black square). Predictions obtained by the ideal liquid phase model (solid lines) and COSMO-RS theoretical curves calculated using the BP_TZVP_21 (dotted lines) (a) and BP_TZVPD_FINE_21 (dashed lines) (b) parametrizations. Results obtained employing the BP_TZVPD_FINE_21 parameters and considering the weight of each conformer calculated from DFTB-MD simulations (dashed-dotted lines) (c). Dihedral distribution function calculated from DFTB-MD simulation of the pure BHA system referred to the dihedral angle shown in the panel (d).

that the agreement between the experimental and theoretical data is far from being satisfactory. This is particularly true for compositions close to the eutectic point, where the employed COSMO model significantly deviates from the experimental data points. In the attempt to better characterize this system, the quantum chemical level was increased; hence, the BP_TZVPD_FINE_21 parametrization was used.[31] The result of this prediction is reported in Figure 2b. Here, the simulated SLE diagram reproduces more accurately the experimental behavior as the experimental melting temperatures are found to lie close to the theoretical lines. As concerns the thermal characterization of this system, both the experimental data points and the COSMO-RS prediction show only a slight MP depression along the phase diagram, and a ΔT_m of 4.0 K is obtained for the eutectic composition (Table S8), highlighting that the thermal behavior of the 4-Met/MEN system is close to the one of an ideal eutectic. To rationalize this result, a useful comparison can be made with a similar system formed by MEN with *p*-cresol (PC), being the latter analogue to the 4-Met molecule but with a methyl group in *para*-position with respect to the hydroxyl, instead of a methoxy moiety.[26] This mixture was previously characterized and showed a marked MP depression for a wide range of compositions, classifying this system by right as a type V DES. At the molecular level, the reason for the different thermal behavior of the 4-Met/MEN mixture can reasonably be searched in the methoxy substituent present in the 4-Met molecule, which, being an electron donor for conjugative effect, reduces the electron delocalization of the hydroxyl oxygen atom. The whole result makes the phenolic oxygen atom a better HBA, thus reducing the polarity asymmetry of this molecule. This enhances the interactions among 4-Met molecules in the pure compound and makes the intermolecular 4-Met−MEN interactions upon mixing less favorable by comparison, which results in a lower deviation from thermodynamic ideality.

Subsequently, the system composed of BHA and MEN was studied and compared to the 4-Met/MEN mixture. The structure of the BHA molecule reminds that of the 4-Met one, except for the functionalization of the aromatic ring via the insertion of a *tert*-butyl (tBu) substituent in *ortho*-position to the hydroxyl group (Figure 1). In Figure 3a,b, we report the SLE diagrams calculated using the COSMO BP_TZVP_21 and BP_TZVPD_FINE_21 parametrization levels, respectively, compared with the ideal phase diagram and the experimental data. Surprisingly, both levels of theory show an unsatisfying agreement with the experimental data. Looking at the structure of the BHA molecule, one may suppose that it can be present in two different forms in the liquid phase (Figure S2), i.e., with the hydroxyl hydrogen atom pointing either toward or to the opposite side of the tBu group (hereafter named *cisoid* and *transoid*, respectively).[65] To estimate the relative abundance of the two rotational conformers, DFTB-MD simulations were carried out on the pristine BHA compound. Subsequently, a dihedral distribution function (DDF) for the dihedral angle (φ) describing the orientation of the hydroxyl group was calculated from DFTB-MD simulations (Figure 3d). By integration of the DDF reported in Figure 3d, the population of the two conformers resulted to be equal to 90% for the *transoid* form and 10% for the *cisoid* one, respectively. The much higher abundance of the *transoid* form is reasonable if one considers the repulsion between the planar O−H group and the protons of the tBu group in the *cisoid* one. To improve the simulated SLE, the weights of the BHA conformers were considered by inserting in the COSMO simulation a *wf* derived from the DDF analysis. Simulating the SLE considering this information resulted in a clear improvement of the phase diagram when compared to

https://doi.org/10.1021/acssuschemeng.3c07965
ACS Sustainable Chem. Eng. XXXX, XXX, XXX−XXX

the experimental data (Figure 3c). This combined approach is thus crucial to characterizing the thermal behavior of mixtures formed by precursors presenting this kind of steric asymmetry. Note that the *transoid* conformer weight was considered to be equal to 99.9% by COSMO calculations performed without the conformer analysis and that neglecting the contribution of the *cisoid* form leads to the overestimation of the MP depression (Figure 3b). This result is reasonable if we consider that the *transoid* rotamer is more suitable to behave as HBD and establish the favorable BHA−MEN donor-receptor interaction, while the same cannot be said for the *cisoid* form. The clear improvement of the SLE prediction deriving from the inclusion of only a small percentage of the *cisoid* rotamer highlights how these calculations are sensitive toward such structural information.

Role of Steric Asymmetry in Addition to Polarity Asymmetry. The thermal behavior evidenced by the BHA/MEN system warrants some further discussion. By comparing the COSMO-simulated phase diagram with the ideal SLE in Figure 3c, one may note that this mixture shows a higher deviation from thermal ideality as compared to the 4-Met/MEN one (Figure 2b), in particular at the eutectic composition (Table S8). However, a methoxy group in the *para*-position to the hydroxyl is present in both the 4-Met and BHA precursors, which can reduce the polarity asymmetry of these molecules. To get further insights into the electrostatic properties of the components, a population analysis on the isolated molecules was carried out from DFT calculations, and the results are shown in Figure S3. As can be observed, the partial charge of the hydroxyl oxygen atom in the MEN molecule is significantly more negative than in the 4-Met and BHA counterparts because of the electron delocalization through the aromatic ring in the latter cases. In addition, the partial charges are comparable for the 4-Met and BHA molecules, confirming their similarity from an electrostatic point of view. Therefore, the different thermal behavior of the BHA/MEN mixture with respect to the 4-Met/MEN one can be reasonably ascribed to only the presence of the tBu substituent in the BHA molecule. Being in one of the two available *ortho*-positions to the hydroxyl, this encumbering group leaves only partial access to the oxygen atom, and significantly reduces the capability of the BHA molecule to act simultaneously as H-bond donor and acceptor. As a result, the intermolecular interactions among BHA molecules in the pure compound are hampered, while the mixed BHA−MEN donor-receptor interaction becomes more favorable upon mixing. A similar effect was previously evidenced by a comparative study on MEN mixtures with butylated hydroxytoluene (BHT), 2-*tert*-butyl-*p*-cresol (TBC), and PC, where TBC and BHT molecules are analogous to the PC one, with respectively one and two tBu groups in *ortho*-position to the hydroxyl.[26] Note that, up to now, the term asymmetric has being used to describe precursors that possess strong HBD but weak HBA sites due to asymmetric polarity, and never to indicate structural or configurational asymmetry.[23] Differently, here, we demonstrate that H-bonding asymmetry due to steric factors from appropriate functionalization of the precursors can also drive the achievement of a type V DES. Considering that both the 4-Met and BHA molecules suffer from a reduced polarity asymmetry, these steric factors appear to be overwhelming with respect to the electrostatic ones.

In the attempt to describe the behavior of the 4-Met and BHA components, one may observe that the methoxy group of these molecules carries a negatively charged oxygen atom that can also act as a potential HBA site. However, the population analysis shows that the methoxy oxygen possesses a considerably less negative partial charge compared to the hydroxyl oxygen in both these molecules (Figure S3), suggesting a scarce involvement in the H-bonding economy. To get further insights into the role of the methoxy group, a useful comparison is offered by the TBEP/MEN system, where the TBEP molecule is analogous to the BHA one, but with an ethyl substituent in the *para*-position to the hydroxyl (Figure 1). Due to the formation of a metastable phase that prevented these mixtures from crystallizing, it was not possible to measure the experimental MP in the range of compositions between x_{TBEP} = 0.3 and x_{TBEP} = 0.7. Under these circumstances, we exploited the predictive capability of our combined COSMO/DFTB-MD approach to get the SLE phase diagram for this mixture, given the reliability of our methodology previously benchmarked against the experimental data. To this purpose, the percentage of conformational rotamers for the TBEP molecule was obtained by integrating the DDF calculated from DFTB-MD simulations of the pristine compound (Figure S4). The SLE calculated using this information is shown in Figure 4 and is compared to the ideal

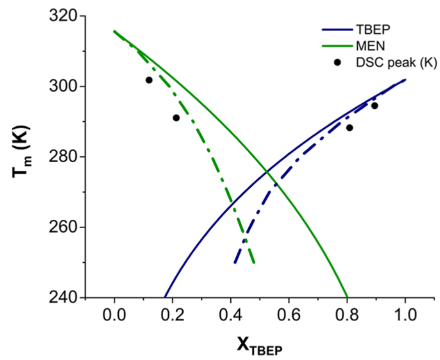

Figure 4. Experimental SLE phase diagram for the TBEP/MEN system measured using the DSC (black circle). Predictions obtained by the ideal liquid phase model (solid lines) and COSMO-RS theoretical curves calculated using the BP_TZVPD_FINE_21 parameters and taking into account the weight of each conformer calculated from DFTB-MD simulations (dashed-dotted lines).

thermal behavior of the mixture. The obtained phase diagram shows a significant deviation from ideality for a considerably wide range of compositions, going from about x_{TBEP} = 0.4−0.6, which is particularly pronounced at the eutectic one (Table S8). Note that, besides having a potential HBA ability, the methoxy group is also capable of reducing the polarity asymmetry of the molecule for the conjugative effect, as previously discussed. However, the population analysis delivers similar partial charges for the BHA and TBEP hydroxyl atoms (Figure S3), suggesting that these molecules are similar from an electrostatic point of view. The whole result, together with the much higher deviation from thermal ideality of the TBEP/MEN mixtures compared to the BHA/MEN mixtures, supports the participation of the methoxy group in the H-bonding activity in the latter case. Indeed, this functionality can enhance the self-aggregation among BHA molecules in the pure state, as the sterically encumbered hydroxyl group can act as H-bond donor toward the methoxy oxygen atom. On the other hand, the hydroxyl group is the only functionality with H-bonding capability in the TBEP molecules, which suffer from a hampered self-aggregation in the pure state. This instance makes much more favorable the interactions with MEN upon mixing and is thus responsible for the higher MP depression of the TBEP/MEN mixtures (Figure 4). Moreover, the result obtained without considering the conformer weight and using both the BP_TZVP_21 and BP_TZVPD_FINE_21 parametrizations (Figure S5) yields a considerably higher deviation from thermal ideality, as previously shown by the BHA/MEN mixture.

Back toward Ideality: TBHQ/MEN Mixtures. With the purpose of understanding the effect of a strong HBD/HBA functionality in the *para*-position on the hydroxyl group, the system composed by TBHQ and MEN was studied. The TBHQ molecule is analogue to the BHA and TBEP precursors, but an additional hydroxyl group is present in *para*-position with respect to the former one, and far from the sterically encumbering tBu moiety (Figure 1). Also in this case, an equilibrium between two rotational conformers is possible; thus, the ratio for the two rotamers was calculated by integrating the DDF derived from DFTB-MD simulations of the pristine compound (Figure S6). The SLE phase diagram calculated considering this information is shown in Figure 5.

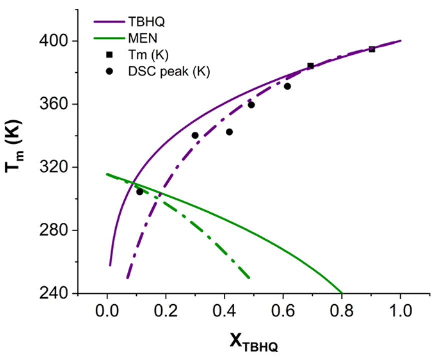

Figure 5. Experimental SLE phase diagram for the TBHQ/MEN system measured using the DSC (black circle) and the visual method (black square). Predictions obtained by the ideal liquid phase model (solid lines) and COSMO-RS theoretical curves calcuated using the BP_TZVPD_FINE_21 parameters and taking into account the weight of each conformer calculated from DFTB-MD simulations (dashed-dotted lines).

Here, one may observe that the simulated curves provide a good description of the experimental melting temperatures. On the other hand, a worst agreement between the theoretical and the experimental results is evidenced without taking into account the obtained conformer population (Figure S7), confirming once more the reliability of our combined approach. The comparison between the COSMO-simulated and the ideal phase diagram shows a lower MP depression with respect to the TBEP/MEN case, in particular, at the eutectic composition (Table S8). Inspection of the partial charges calculated for the TBHQ molecule (Figure S3) delivers the reason for this thermal behavior. In fact, the oxygen atom of the sterically free hydroxyl group displays a particularly negative charge (−0.60), more negative than the one associated with the hydroxyl group in the *ortho*-position to the tBu. Consequently, it is reasonable to assume that a considerable amount of the H-bonding activity played by the TBHQ molecule is driven by this functional group in addition to the sterically hindered hydroxyl. In this way, the H-bonding asymmetry due to steric factors given by the tBu group is partially annulled and the TBHQ species can behave simultaneously as strong HBD and HBA in the pure form. This leads to a return toward thermodynamic ideality, corroborating our findings about the steric contribution in these systems.

■ CONCLUSIONS

A comprehensive study about the thermal behavior of the hydrophobic eutectic mixtures formed by MEN with different counterparts, namely, 4-Met, BHA, TBEP, and TBHQ, was carried out with the aim of enlightening the different contributions at the molecular level able to provide a type V DES. The chosen systems allowed us to disentangle the electrostatic and structural factors governing the H-bonding asymmetry of the mixture precursors, i.e., the capability to act as strong HBD and weak HBA or vice versa. The SLE phase diagram calculations significantly benefit from the inclusion of the relative abundance of the different rotational conformers describing the BHA, TBEP, and TBHQ precursors, while neglecting this contribution results in an overestimation of the MP depression. This structural information was obtained by DFTB-MD simulations and included in the COSMO-RS calculations with a combined approach presented here for the first time. Having validated this protocol against the experimental data when available, we exploited its predictive capability to obtain information about the solid−liquid equilibrium despite the lack of experimental data, as in case of the TBEP/MEN mixtures.

The SLE phase diagram obtained for the 4-Met/MEN mixture shows a behavior close to thermodynamic ideality. This is due to the electrostatic properties of the 4-Met molecule, which, carrying a methoxy substituent in the *para*-position to the hydroxyl group, sees a reduction of its polarity asymmetry, at variance with other phenolic compounds. This results in an enhanced self-interaction among 4-Met molecules in the pure state and a low deviation from ideality upon mixing with MEN. These electrostatic effects are bypassed by the insertion of a tBu substituent in the *ortho*-position to the hydroxyl group in the BHA molecule, highlighting the dominating role of the steric factors over the electrostatic ones on the thermal properties of these mixtures. The steric encumbrance hinders the hydroxyl oxygen atom and hampers the contemporary H-bond donor/acceptor capabilities of the BHA molecule, reducing the self-aggregation in the pristine compound and providing a higher deviation from thermal ideality upon mixing with MEN. An even higher MP depression is evidenced by the TBEP/MEN mixtures, where the TBEP molecule is analogous to the BHA one but with an ethyl substituent in the *para*-position to the hydroxyl instead than a methoxy moiety. Finally, the presence of an additional sterically free hydroxyl group with strong HBD/HBA capabilities in the TBHQ molecule leads the TBHQ/MEN mixtures back toward thermodynamic ideality and corroborates our findings.

In this way, the peculiarity of the precursor molecules allowed us to elucidate the fine balance between the different contributions ruling the thermal behavior of these mixtures in great detail. The impact of this work is that of providing new tools for the prediction of the thermal properties of type V DES, and new insights for a more conscious design of these tunable solvents.

https://doi.org/10.1021/acssuschemeng.3c07965
ACS Sustainable Chem. Eng. XXXX, XXX, XXX−XXX

ASSOCIATED CONTENT

Supporting Information

The Supporting Information is available free of charge at https://pubs.acs.org/doi/10.1021/acssuschemeng.3c07965.

List of the prepared samples, details of the simulated DFTB-MD systems, parameters employed in the COSMO-RS calculations, and additional results (PDF)

AUTHOR INFORMATION

Corresponding Authors

João A. P. Coutinho − *CICECO, Aveiro Institute of Materials, Complexo de Laboratórios Tecnológicos, University of Aveiro, 3810-193 Aveiro, Portugal*; orcid.org/0000-0002-3841-743X; Email: jcoutinho@ua.pt

Paola D'Angelo − *Department of Chemistry, University of Rome 'La Sapienza', 00185 Rome, Italy*; orcid.org/0000-0001-5015-8410; Email: p.dangelo@uniroma1.it

Authors

Giorgia Mannucci − *Department of Chemistry, University of Rome 'La Sapienza', 00185 Rome, Italy*; orcid.org/0000-0002-6170-3522

Gabriel Teixeira − *CICECO, Aveiro Institute of Materials, Complexo de Laboratórios Tecnológicos, University of Aveiro, 3810-193 Aveiro, Portugal*; orcid.org/0000-0002-5213-5359

Filipe Hobi Bordon Sosa − *CICECO, Aveiro Institute of Materials, Complexo de Laboratórios Tecnológicos, University of Aveiro, 3810-193 Aveiro, Portugal*

Matteo Palluzzi − *Department of Chemistry, University of Rome 'La Sapienza', 00185 Rome, Italy*

Matteo Busato − *Department of Chemistry, University of Rome 'La Sapienza', 00185 Rome, Italy*; orcid.org/0000-0002-9450-0481

Complete contact information is available at:
https://pubs.acs.org/10.1021/acssuschemeng.3c07965

Author Contributions

The manuscript was written through contributions of all authors. All authors have given approval to the final version of the manuscript.

Notes

The authors declare no competing financial interest.

ACKNOWLEDGMENTS

The authors acknowledge the European Union-NextGenerationEU under the Italian Ministry of University and Research (MUR), Network 4 Energy Sustainable Transition—NEST project (MIUR project code PE000021, Concession Degree no. 1561 of October 11, 2022)—CUP C93C22005230007. This work was partially developed within the scope of the project CICECO-Aveiro Institute of Materials, UIDB/50011/2020, UIDP/50011/2020, and LA/P/0006/2020, financed by national funds through the FCT/MCTES (PIDDAC). G.T. thanks FCT for his Ph.D. grant (UI/BD/151114/2021). F.H.B.S. acknowledges FCT—Fundação para a Ciência e a Tecnologia, I.P. for the researcher contract CEECIND/07209/2022, under the Scientific Employment Stimulus-Individual Call.

REFERENCES

(1) Hansen, B. B.; Spittle, S.; Chen, B.; Poe, D.; Zhang, Y.; Klein, J. M.; Horton, A.; Adhikari, L.; Zelovich, T.; Doherty, B. W.; Gurkan, B.; Maginn, E. J.; Ragauskas, A.; Dadmun, M.; Zawodzinski, T. A.; Baker, G. A.; Tuckerman, M. E.; Savinell, R. F.; Sangoro, J. R. Deep Eutectic Solvents: A Review of Fundamentals and Applications. *Chem. Rev.* **2021**, *121* (3), 1232−1285.

(2) Francisco, M.; den Bruinhorst, A.; Kroon, M. C. Low-Transition-Temperature Mixtures (LTTMs): A New Generation of Designer Solvents. *Angew. Chem., Int. Ed.* **2013**, *52*, 3074−3085.

(3) Smith, E. L.; Abbott, A. P.; Ryder, K. S. Deep Eutectic Solvents (DESs) and Their Applications. *Chem. Rev.* **2014**, *114* (21), 11060−11082.

(4) Schaeffer, N.; Conceição, J. H. F.; Martins, M. A. R.; Neves, M. C.; Pérez-Sánchez, G.; Gomes, J. R. B.; Papaiconomou, N.; Coutinho, J. A. P. Non-Ionic Hydrophobic Eutectics − Versatile Solvents for Tailored Metal Separation and Valorisation. *Green Chem.* **2020**, *22*, 2810−2820.

(5) Schaeffer, N.; Martins, M. A. R.; Neves, C. M. S. S.; Pinho, S. P.; Coutinho, J. A. P. Sustainable Hydrophobic Terpene-Based Eutectic Solvents for the Extraction and Separation of Metals. *Chem. Commun.* **2018**, *54*, 8104−8107.

(6) Ribeiro, B. D.; Florindo, C.; Iff, L. C.; Coelho, M. A. Z.; Marrucho, I. M. Menthol-Based Eutectic Mixtures: Hydrophobic Low Viscosity Solvents. *ACS Sustain. Chem. Eng.* **2015**, *3*, 2469−2477.

(7) Dal Bosco, C.; Mariani, F.; Gentili, A. Hydrophobic Eutectic Solvent-Based Dispersive Liquid-Liquid Microextraction Applied to the Analysis of Pesticides in Wine. *Molecules* **2022**, *27*, 908.

(8) Busato, M.; Di Lisio, V.; Del Giudice, A.; Tomai, P.; Migliorati, V.; Galantini, L.; Gentili, A.; Martinelli, A.; D'Angelo, P. Transition from Molecular- to Nano-Scale Segregation in a Deep Eutectic Solvent - Water Mixture. *J. Mol. Liq.* **2021**, *331*, No. 115747.

(9) Tang, W.; Dai, Y.; Row, K. Evaluation of Fatty Acid/Alcohol-Based Hydrophobic Deep Eutectic Solvents as Media for Extracting Antibiotics from Environmental Water. *Anal. Bioanal. Chem.* **2018**, *410*, 7325−7336.

(10) Murakami, Y.; Das, S. K.; Himuro, Y.; Maeda, S. Triplet-Sensitized Photon Upconversion in Deep Eutectic Solvents. *Phys. Chem. Chem. Phys.* **2017**, *19*, 30603−30615.

(11) Cruz, H.; Jordão, N.; Amorim, P.; Dionísio, M.; Branco, L. C. Deep Eutectic Solvents as Suitable Electrolytes for Electrochromic Devices. *ACS Sustain. Chem. Eng.* **2018**, *6*, 2240−2249.

(12) Abbott, A. P.; Capper, G.; Davies, D. L.; Rasheed, R. K.; Archer, J.; John, C. Electrodeposition of Chromium Black from Ionic Liquids. *Inst. Met. Finish.* **2004**, *82* (1−2), 14−17.

(13) Danilov, F. I.; Protsenko, V. S.; Kityk, A. A.; Shaiderov, D. A.; Vasil'Eva, E. A.; Kumar, U. P.; Kennady, C. J. Electrodeposition of Nanocrystalline Nickel Coatings from a Deep Eutectic Solvent with Water Addition. *Prot. Met.* **2017**, *53*, 1131−1138.

(14) Busato, M.; Tofoni, A.; Mannucci, G.; Tavani, F.; Del Giudice, A.; Colella, A.; Giustini, M.; D'Angelo, P. On the Role of Water in the Formation of a Deep Eutectic Solvent Based on $NiCl_2·6H_2O$ and Urea. *Inorg. Chem.* **2022**, *61* (23), 8843−8853.

(15) Milker, S.; Pätzold, M.; Bloh, J. Z.; Holtmann, D. Comparison of Deep Eutectic Solvents and Solvent-Free Reaction Conditions for Aldol Production. *Mol. Catal.* **2019**, *466*, 70−74.

(16) Abbott, A. P.; Bell, T. J.; Handa, S.; Stoddart, B. O-Acetylation of Cellulose and Monosaccharides Using a Zinc Based Ionic Liquid. *Green Chem.* **2005**, *7*, 705−707.

(17) Arnaboldi, S.; Mezzetta, A.; Grecchi, S.; Longhi, M.; Emanuele, E.; Rizzo, S.; Arduini, F.; Micheli, L.; Guazzelli, L.; Mussini, P. R. Natural-Based Chiral Task-Specific Deep Eutectic Solvents: A Novel, Effective Tool for Enantiodiscrimination in Electroanalysis. *Electrochim. Acta* **2021**, *380*, No. 138189.

(18) Shi, M.; Xiong, W.; Tu, Z.; Zhang, X.; Hu, X.; Wu, Y. Task-Specific Deep Eutectic Solvents for the Highly Efficient and Selective Separation of H_2. *Sep. Purif. Technol.* **2021**, *276*, No. 119357.

(19) Busato, M.; Del Giudice, A.; Di Lisio, V.; Tomai, P.; Migliorati, V.; Gentili, A.; Martinelli, A.; D'Angelo, P. Fate of a Deep Eutectic

Solvent upon Cosolvent Addition: Choline Chloride-Sesamol 1:3 Mixtures with Methanol. *ACS Sustain. Chem. Eng.* **2021**, *9*, 12252−12261.

(20) Mannucci, G.; Busato, M.; Tofoni, A.; D'Angelo, P. Structural Evolution of the Butylated Hydroxytoluene/Menthol Hydrophobic Eutectic Solvent upon Methanol and Ethanol Cosolvent Addition. *J. Mol. Liq.* **2023**, *375*, No. 121302.

(21) Van Osch, D. J. G. P.; Dietz, C. H. J. T.; Warrag, S. E. E.; Kroon, M. C. The Curious Case of Hydrophobic Deep Eutectic Solvents: A Story on the Discovery, Design, and Applications. *ACS Sustain. Chem. Eng.* **2020**, *8*, 10591−10612.

(22) Van Osch, D. J. G. P.; Zubeir, L. F.; van den Bruinhorst, A.; Rocha, M. A. A.; Kroon, M. C. Hydrophobic Deep Eutectic Solvents as Water-Immiscible Extractants. *Green Chem.* **2015**, *17*, 4518−4521.

(23) Abranches, D. O.; Coutinho, J. A. P. Type V Deep Eutectic Solvents: Design and Applications. *Curr. Opin. Green Sustain. Chem.* **2022**, *35*, No. 100612.

(24) Abbott, A. P.; Capper, G.; Davies, D. L.; Rasheed, R. K.; Tambyrajah, V. Novel Solvent Properties of Choline Chloride/Urea Mixtures. *Chem. Commun.* **2003**, *1*, 70−71.

(25) Martins, M. A. R.; Pinho, S. P.; Coutinho, J. A. P. Insights Into the Nature of Eutectic and Deep Eutectic Mixtures. *J. Solution Chem.* **2019**, *48*, 962−982.

(26) Busato, M.; Mannucci, G.; Rocchi, L. A.; Di Pietro, M. E.; Capocefalo, A.; Zorzi, E.; Casu, P.; Veclani, D.; Castiglione, F.; Mele, A.; Martinelli, A.; Postorino, P.; D'Angelo, P. The Complex Story Behind a Deep Eutectic Solvent Formation as Revealed by L-Menthol Mixtures with Butylated Hydroxytoluene Derivatives. *ACS Sustain. Chem. Eng.* **2023**, *11*, 8988−8999.

(27) Busato, M.; Migliorati, V.; Del Giudice, A.; Di Lisio, V.; Tomai, P.; Gentili, A.; D'Angelo, P. Anatomy of a Deep Eutectic Solvent: Structural Properties of Choline Chloride:Sesamol 1:3 Compared to Reline. *Phys. Chem. Chem. Phys.* **2021**, *23* (20), 11746−11754.

(28) Schaeffer, N.; Abranches, D. O.; Silva, L. P.; Martins, M. A. R.; Carvalho, P. J.; Russina, O.; Triolo, A.; Paccou, L.; Guinet, Y.; Hedoux, A. Non-Ideality in Thymol+Menthol Type V Deep Eutectic Solvents. *ACS Sustain. Chem. Eng.* **2021**, *9*, 2203−2211.

(29) Abranches, D. O.; Martins, M. A. R.; Silva, L. P.; Schaeffer, N.; Pinho, S. P.; Coutinho, J. A. P. Phenolic Hydrogen Bond Donors in the Formation of Non-Ionic Deep Eutectic Solvents: The Quest for Type V DES. *Chem. comm.* **2019**, *55* (69), 10253−10256.

(30) Alhadid, A.; Jandl, C.; Mokrushina, L.; Minceva, M. Nonideality and Cocrystal Formation in L-Menthol/Xylenol Eutectic Systems. *J. Mol. Liq.* **2022**, *367*, No. 120582.

(31) Teixeira, G.; Abranches, D. O.; Ferreira, O.; Coutinho, J. A. P. Estimating the Melting Temperatures of Type V Deep Eutectic Solvents. *Ind. Eng. Chem. Res.* **2023**, *62* (36), 14638−14647.

(32) Teixeira, G.; Abranches, D. O.; Silva, L. P.; Vilas-Boas, S. M.; Pinho, S. P.; Ferreira, A. I.; Santos, L. M.; Ferreira, O.; Coutinho, J. A. P. Liquefying Flavonoids with Terpenoids through Deep Eutectic Solvent Formation. *Molecules* **2022**, *27*, 2649.

(33) Abranches, D. O.; Coutinho, J. A. P. Everything You Wanted to Know about Deep Eutectic Solvents but Were Afraid to Be Told. *Annu. Rev. Chem. Biomol Eng.* **2023**, *14*, 141−163.

(34) Klamt, A. The COSMO and COSMO-RS Solvation Models. *Wiley Interdiscip. Rev. Comput. Mol. Sci.* **2018**, *8*, No. e1338.

(35) Wang, S.; Sandler, S. I.; Chen, C.-C. Refinement of COSMO-SAC and the Applications. *Ind. Eng. Chem. Res.* **2007**, *46*, 7275−7288.

(36) Klamt, A. Conductor-like Screening Model for Real Solvents: A New Approach to the Quantitative Calculation of Solvation Phenomena. *J. Phys. Chem.* **1995**, *99* (7), 2224−2235.

(37) Klamt, A.; Jonas, V.; Bürger, T.; Lohrenz, J. C. W. Refinement and Parametrization of COSMO-RS. *J. Phys. Chem. A* **1998**, *102* (26), 5074−5085.

(38) Kovács, A.; Neyts, E. C.; Cornet, I.; Wijnants, M.; Billen, P. Modeling the Physicochemical Properties of Natural Deep Eutectic Solvents. *ChemSusChem* **2020**, *13* (15), 3789−3804.

(39) Busato, M.; Mannucci, G.; Di Lisio, V.; Martinelli, A.; Del Giudice, A.; Tofoni, A.; Dal Bosco, C.; Migliorati, V.; Gentili, A.; D'Angelo, P. Structural Study of a Eutectic Solvent Reveals Hydrophobic Segregation and Lack of Hydrogen Bonding between the Components. *ACS Sustain. Chem. Eng.* **2022**, *10*, 6337−6345.

(40) *TURBOMOLE V4.5.2, a Development of University of Karlsruhe and Forschungszentrum Karlsruhe GmbH, 1989−2007*; TURBOMOLE GmbH, 2007, https://www.turbomole.org (accessed June 12, 2023).

(41) Perdew, J. P. Density-Functional Approximation for the Correlation Energy of the Inhomogeneous Electron Gas. *Phys. Rev. B* **1986**, *33* (12), 8822.

(42) Becke, A. D. Density-Functional Exchange-Energy Approximation with Correct Asymptotic Behavior. *Phys. Rev. A* **1988**, *38* (6), 3098.

(43) Schäfer, A.; Huber, C.; Ahlrichs, R. Fully Optimized Contracted Gaussian Basis Sets of Triple Zeta Valence Quality for Atoms Li to Kr. *J. Chem. Phys.* **1994**, *100* (8), 5829−5835.

(44) Weigend, F.; Häser, M.; Patzelt, H.; Ahlrichs, R. RI-MP2: Optimized Auxiliary Basis Sets and Demonstration of Efficiency. *Chem. Phys. Lett.* **1998**, *294* (1−3), 143−152.

(45) Weigend, F.; Ahlrichs, R. Balanced Basis Sets of Split Valence, Triple Zeta Valence and Quadruple Zeta Valence Quality for H to Rn: Design and Assessment of Accuracy. *Phys. Chem. Chem. Phys.* **2005**, *7* (18), 3297−3305.

(46) *BIOVIACOSMOtherm*; DassaultSystèmes, 2021, https://www.3ds.com/products/biovia/cosmo-rs/cosmotherm (accessed June 12, 2023)

(47) Gaus, M.; Cui, Q.; Elstner, M. DFTB3: Extension of the Self-Consistent-Charge Density-Functional Tight-Binding Method (SCC-DFTB). *J. Chem. Theory Comput.* **2011**, *7*, 931−948.

(48) Christensen, A. S.; Kubař, T.; Cui, Q.; Elstner, M. Semiempirical Quantum Mechanical Methods for Noncovalent Interactions for Chemical and Biochemical Applications. *Chem. Rev.* **2016**, *116* (9), 5301−5337.

(49) Christensen, A. S.; Elstner, M.; Cui, Q. Improving Intermolecular Interactions in DFTB3 Using Extended Polarization from Chemical-Potential Equalization. *J. Chem. Phys.* **2015**, *143* (8), No. 084123.

(50) Hourahine, B.; Aradi, B.; Blum, V.; Bonafé, F.; Buccheri, A.; Camacho, C.; Cevallos, C.; Deshaye, M. Y.; Dumitric, T.; Dominguez, A.; Ehlert, S.; Elstner, M.; Van Der Heide, T.; Hermann, J.; Irle, S.; Kranz, J. J.; Köhler, C.; Kowalczyk, T.; Kubař, T.; Lee, I. S.; Lutsker, V.; Maurer, R. J.; Min, S. K.; Mitchell, I.; Negre, C.; Niehaus, T. A.; Niklasson, A. M. N.; Page, A. J.; Pecchia, A.; Penazzi, G.; Persson, M. P.; Řezáč, J.; Sánchez, C. G.; Sternberg, M.; Stöhr, M.; Stuckenberg, F.; Tkatchenko, A.; Yu, V. W. Z.; Frauenheim, T. DFTB+, a Software Package for Efficient Approximate Density Functional Theory Based Atomistic Simulations. *J. Chem. Phys.* **2020**, *152* (12), 124101.

(51) Gaus, M.; Goez, A.; Elstner, M. Parametrization and Benchmark of DFTB3 for Organic Molecules. *J. Chem. Theory Comput.* **2013**, *9* (1), 338−354.

(52) Martínez, L.; Andrade, R.; Birgin, E. G.; Martínez, J. M. Software News and Update Packmol: A Package for Building Initial Configurations for Molecular Dynamics Simulations. *J. Comput. Chem.* **2009**, *30*, 2157−2164.

(53) Caldeweyher, E.; Ehlert, S.; Hansen, A.; Neugebauer, H.; Spicher, S.; Bannwarth, C.; Grimme, S. A Generally Applicable Atomic-Charge Dependent London Dispersion Correction. *J. Chem. Phys.* **2019**, *150* (15), 154122.

(54) Abraham, M. J.; Murtola, T.; Schulz, R.; Páll, S.; Smith, J. C.; Hess, B.; Lindahl, E. GROMACS: High Performance Molecular Simulations through Multi-Level Parallelism from Laptops to Supercomputers. *SoftwareX* **2015**, *1*, 19−25.

(55) Jorgensen, W. L.; Maxwell, D. S.; Tirado-Rives, J. Development and Testing of the OPLS All-Atom Force Field on Conformational Energetics and Properties of Organic Liquids. *J. Am. Chem. Soc.* **1996**, *118*, 11225−11236.

(56) Darden, T.; York, D.; Pedersen, L. Particle Mesh Ewald: An Nlog (N) Method for Ewald Sums in Large Systems. *J. Chem. Phys.* **1993**, *98*, 10089−10092.

(57) Essmann, U.; Perera, L.; Berkowitz, M. L.; Darden, T.; Lee, H.; Pedersen, L. G. A Smooth Particle Mesh Ewald Method. *J. Chem. Phys.* **1995**, *103*, 8577−8593.

(58) Hess, B.; Bekker, H.; Berendsen, H. J. C.; Fraaije, J. G. E. M. LINCS: A Linear Constraint Solver for Molecular Simulations. *J. Comput. Chem.* **1997**, *18*, 1463−1472.

(59) Breneman, C. M.; Wiberg, K. B. Determining Atom-Centered Monopoles from Molecular Electrostatic Potentials. The Need for High Sampling Density in Formamide Conformational Analysis. *J. Comput. Chem.* **1990**, *11* (3), 361−373.

(60) Becke, A. D.; Density-Functional Thermochemistry, I. The Effect of the Exchange-Only Gradient Correction. *J. Chem. Phys.* **1992**, *96* (3), 2155−2160.

(61) Frisch, M. J.; Trucks, G. W.; Schlegel, H. B.; Scuseria, G. E.; Robb, M. A.; Cheeseman, J. R.; Scalmani, G.; Barone, V.; Petersson, G. A.; Nakatsuji, H.; Li, X.; Caricato, M.; Marenich, A. V; Bloino, J.; Janesko, B. G.; Gomperts, R.; Mennucci, B.; Hratchian, H. P.; Ortiz, J. V; Izmaylov, A. F.; Sonnenberg, J. L.; Williams-Young, D.; Ding, F.; Lipparini, F.; Egidi, F.; Goings, J.; Peng, B.; Petrone, A.; Henderson, T.; Ranasinghe, D.; Zakrzewski, V. G.; Gao, J.; Rega, N.; Zheng, G.; Liang, W.; Hada, M.; Ehara, M.; Toyota, K.; Fukuda, R.; Hasegawa, J.; Ishida, M.; Nakajima, T.; Honda, Y.; Kitao, O.; Nakai, H.; Vreven, T.; Throssell, K.; Montgomery, Jr., J. A.; Peralta, J. E.; Ogliaro, F.; Bearpark, M. J.; Heyd, J. J.; Brothers, E. N.; Kudin, K. N.; Staroverov, V. N.; Keith, T. A.; Kobayashi, R.; Normand, J.; Raghavachari, K.; Rendell, A. P.; Burant, J. C.; Iyengar, S. S.; Tomasi, J.; Cossi, M.; Millam, J. M.; Klene, M.; Adamo, C.; Cammi, R.; Ochterski, J. W.; Martin, R. L.; Morokuma, K.; Farkas, O.; Foresman, J. B.; Fox, D. J. *Gaussian 16 Revision C.01*; Gaussian, Inc.: 2016.

(62) Abranches, D. O.; Larriba, M.; Silva, L. P.; Melle-Franco, M.; Palomar, J. F.; Pinho, S. P.; Coutinho, J. A. P. Using COSMO-RS to Design Choline Chloride Pharmaceutical Eutectic Solvents. *Fluid Ph. Equilibria* **2019**, *497*, 71−78.

(63) Freire, M. G.; Ventura, S. P. M.; Santos, L. M. N. B. F.; Marrucho, I. M.; Coutinho, J. A. P. Evaluation of COSMO-RS for the Prediction of LLE and VLE of Water and Ionic Liquids Binary Systems. *Fluid Ph. Equilibria* **2008**, *268* (1−2), 74−84.

(64) Song, Z.; Wang, J.; Sundmacher, K. Evaluation of COSMO-RS for Solid−Liquid Equilibria Prediction of Binary Eutectic Solvent Systems. *GEE* **2021**, *6* (3), 371−379.

(65) Lin-Vien, D.; Colthup, N. B.; Fateley, W. G.; Grasselli, J. G. The Handbook of Infrared and Raman Characteristic Frequencies of Organic Molecules. *Elsevier* **1991**, 45−60.

https://doi.org/10.1021/acssuschemeng.3c07965
ACS Sustainable Chem. Eng. XXXX, XXX, XXX−XXX